Environ. Water Eng., 2025, 11(4), 574-485 https://doi.org/10.22034/ewe.2025.537171.2045

EWE

Environment and Water Engineering

Homepage: www.jewe.ir

ISSN: 2476-3683

Laboratory investigation of the application of semi-circular rotary gate within a rectangular canal

Mehrdad Kheiraie[1], Hojatollah Yonesi[1]✉, Babak Shahinejad[1], Hassan Torabipoodeh[1], and Ava Marashi[1]

[1]Water Engineering Department, Faculty of Agriculture, Lorestan University, Khoramabad, Iran

ARTICLE INFO

Paper Type: Research Paper

Received: 26 July 2025
Revised: 21 September 2025
Accepted: 26 September 2025
Published: 28 September 2025

Keywords
Discharge Coefficient
Free Flow
Gradually Transition
Rotary Gate
Stage-Discharge

Corresponding author:
H. Yonesi
✉ yonesi.h@lu.ac.ir

ABSTRACT

This study aimed to evaluate the hydraulic performance of a semi-circular rotary gate in a rectangular canal, focusing on the effects of gate opening angles and gradually transition lengths on flow behavior, including discharge and discharge coefficient. To accommodate the gate, the canal cross-section gradually shifted from rectangular to semi-circular over three transition lengths: 0.6, 0.9, and 1.2 m. Laboratory experiments were conducted under varying flow rates, upstream water depths, and gate openings in free-flow conditions. The discharge coefficient increased with larger gate openings but decreased as transition length increased. Two discharge estimation equations were developed, with the dimensional analysis approach providing more accurate predictions than the conventional stage–discharge method. Ignoring transition length in simplified calculations led to significant errors. The discharge coefficient varied with gate opening angle: 0.18–1.35 for 0.6 m, 0.17–1.29 for 0.9 m, and 0.15–1.23 for 1.2 m transitions. The proposed equations reliably predicted discharge, with experimental and computational results showing a mean error below 5%. These findings highlight the critical role of including transition length in design calculations for accurate performance assessment of semi-circular rotary gates in irrigation systems.

Highlights

- Accurate measurement of water discharge to the farm for proper water resource management.
- Due to the neutralization of the water flow resistance on both sides of the gate, the operator can easily use it.
- A gradual transition structure from a rectangular cross-section to a semi-circle reduces the energy loss.
- The obtained relationships can be programmed by the computer to pass a specific flow through the canal

Citing:
Kheiraie, M., Yonesi, H. A., Shahinejad, B., Torabipoudeh, H., & Maraashi, A. (2025). Laboratory investigation of the application of semi-circular rotary gate within a rectangular canal. *Environment and Water Engineering*, *11*(4), 574-585. https://doi.org/10.22034/ewe.2025.537171.2045

1. Introduction

Accurate flow measurement and control are crucial for managing irrigation and water supply. Flow control structures like sluices and radial gates regulate water discharge and depth, enabling precise measurement. Sluice gates are common in irrigation, with extensive research on their hydraulics, stage-discharge relationships, and discharge coefficients. Swamee (1992) used non-linear regression for canal flow regulation, Vanden-Broeck (1997) and Daneshfaraz et al. (2016) applied numerical solutions of the mixed potential function, and Kim (2007) used Navier-Stokes equations to study flow compressibility and hydraulic jumps. Belaud et al. (2009) refined predictions via energy and momentum equations. Operational challenges of sluice gates include gate weight and friction, making operation slow. Radial gates, though costlier, offer alternatives. Bijankhan et al. (2013) improved radial gate calibration using dimensional analysis and incomplete self-similarity. Salmasi and Abraham (2020) studied inclined slide gates, showing higher discharge coefficients with increased gate angles. Khalili Shayan et al. (2021) developed energy- and momentum-based methods to estimate gate openings, reducing errors. Meng et al. (2024) examined trapezoidal gates, highlighting scale effects, while

Hashem et al. (2024) studied triangular gates, showing efficiency gains based on geometry and operation mode. Hydraulic performance is categorized into free and submerged flow, affecting discharge coefficients and emphasizing precise gate operation. Gharibreza et al. (2018) used a combination of coastal sedimentology, satellite imagery, GIS (ArcGIS 10.1), and MIKE-21 simulations to analyze sea-level-driven sedimentary changes and shoreline dynamics in the GB. Recent studies refined sluice gate performance further. Rojas (2020) benchmarked submerged gate calibration, finding dimensional analysis methods accurate within ±3%, versus ±40% errors for constant coefficient methods. Lauria et al. (2020) linked discharge coefficients to gate opening, wall slope, and side contraction. Wang and Diao (2021) derived formulas for small openings (<0.10), noting inflection around 0.04. Daneshfaraz et al. (2022) showed sills affect discharge coefficients by 5–15%. Dehghani et al. (2023) studied U-shaped gates, showing coefficients of 0.35–0.7 depending on geometry, Froude number, and upstream depth.

More recently, rotary gates, especially in semi-circular or semi-elliptical canals, have been proposed and tested as a type of flow control gate. This gate offers several advantages over conventional gates, including rotation about a vertical axis, minimal force and time needed to operate, less interference with sediment and debris, and flexibility in geometric sections. Under free flow, relationships between opening angles, flow depths, and discharge coefficients have been established by Marashi et al. (2021a). Under submerged conditions, Marashi et al. (2021b) analyzed submerged discharge for rotary gates, finding that opening angle and submergence ratio are among the most influential parameters, and proposed threshold criteria for submerged flow. Recent experimental work by Marashi et al. (2021a,b) analyzed how gate opening angle affects discharge coefficient and flow depth in both free and submerged hydraulic jump conditions. In addition, Marashi et al. (2023) applied machine learning and intelligent models to rotary gate discharge estimation, demonstrating improvements in prediction across both free and submerged flow regimes over deterministic methods.

The following benefits can be mentioned regarding the use of rotary gates in irrigation networks: ease of maneuverability due to rotational movement around a vertical axis, the need for very little force during maneuvering, the minimal time required to transition from minimum to maximum opening, the absence of issues with the accumulation of floating materials and sediments behind the structure and the ability to be applied in all geometric cross-sections (Marashi et al. (2019)). This gate does not require sealing during operation. However, for a completely closed position, sealing strips in the shape of an arc (approximately a quarter circle) can be installed on either side of the transition wall (where the gate is located). These strips are aligned along the axis of the gate, one downstream (on the side where the gate rotates upward) and the other upstream (on the side where the gate rotates downward). This ensures that a complete seal is achieved when the gate is fully closed. By describing this structure relatively comprehensively as a gate with a new geometry for regulating the flow level and measuring the discharge, this research investigates the hydraulics of a semi-circular rotary gate in a rectangular canal. The main objective of this study is to comprehensively investigate the hydraulic performance of the semi-circular rotary gate through experimental observations and detailed analyses in a rectangular canal. The innovation of this research lies in introducing a gate with a unique rotational mechanism that requires minimal force to operate, prevents the accumulation of sediments and debris, and can be applied in various geometric cross-sections. Additionally, the study incorporates the innovative use of a gradual transition from a rectangular to a semi-circular cross-section, enabling the practical implementation of semi-circular rotary gates in conventional rectangular canals. Furthermore, this study develops precise discharge coefficient relationships and examines the effects of free flow conditions, which contribute to improved flow regulation and water management in irrigation systems.

2. Materials and methods

2.1 Physical model

A rectangular canal made of Plexiglas with 12 m length, 0.6 m width, and a longitudinal slope of 0.00088 is constructed in the Water Research Laboratory of the Water Engineering Department at Lorestan University, Iran. A centrifugal pump with a maximum nominal discharge of 53 l/s delivers flow from an underground tank to a fixed-height head tank. The flow is adjusted by the gate to the required value in each experiment. Excess flow from the head tank is recirculated through a pipe to the underground tank. The flow depth was measured using a point gauge with an accuracy of 0.0001 m, and the flow rate was measured by an electromagnetic flow meter with an accuracy of 0.00001 m^3/s installed on the inlet pipe of the canal feeder. To reduce errors in the depth measurements, water depth was measured at three different sections across the canal width. A hinged gate of the same size as the canal width was installed at the end of the canal and was used to regulate the water level and obtain the required depth during the experiments. A galvanized sheet with a thickness of 0.0004 m was employed to create a gradual transition from a rectangular to a semi-circular cross-section. The length of these transitions was 0.6, 0.9, and 1.2 m, respectively. The transition set and rotary gate are installed at a distance of 6 m from the upstream of the canal. The upper part of each transition was connected to the walls and floor of the canal upstream, and the lower part was attached to a semi-circular frame with a diameter of 0.6 meters at the gate location. It should be noted that the semi-circle section continued for 0.3 meters downstream from the transfer section (equal to the radius of the gate). Fig. 1 provides a schematic diagram of the transition described. The semi-circular rotary gate was made from a 2 mm-thick iron sheet. This gate was installed at the downstream end of the transition, where the cross-section of the canal becomes semi-circular. The photographs of the construction and installation of the transition and rotary gate in the canal are shown in Fig. 2. It should be noted that a graded ring was used to adjust the position of the rotary gate concerning the transverse direction of the canal.

Fig. 1 Schematic of the gradual transition from a rectangular canal to a semi-circular section: *a*) 3D view, *b*) top view, *c*) front view, and *d*) rear view

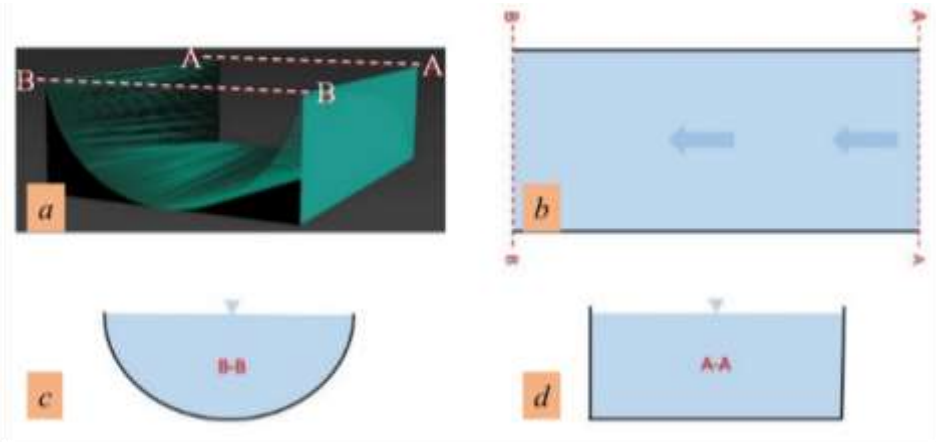

Fig. 2 Installation process of the rotary gate and transition: *a*) gradual transition, *b*) rotary gate, and *c*) graded ring

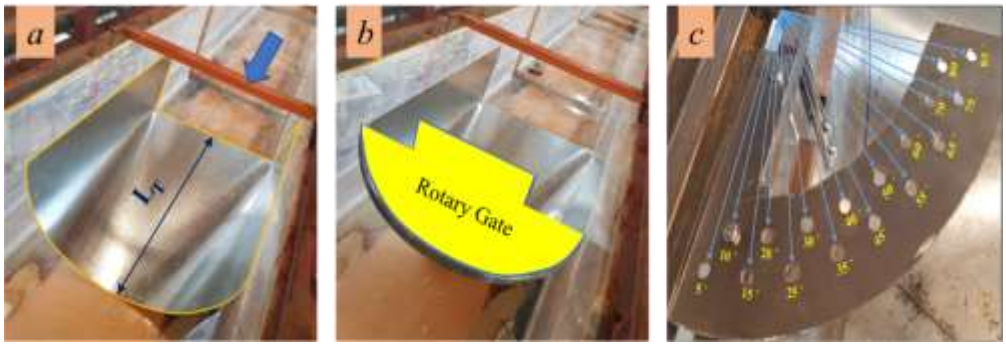

Fig. 3 shows the locations where flow depth measurements were taken and water level profiles were recorded during the experiments and the downstream side of the gate under free-flow conditions.

Fig. 3: a) Flow-depth measurement points along canal length and width; (b–d) collision of two outflows at L_T = 0.6, 0.9, and 1.2 m under free-flow conditions

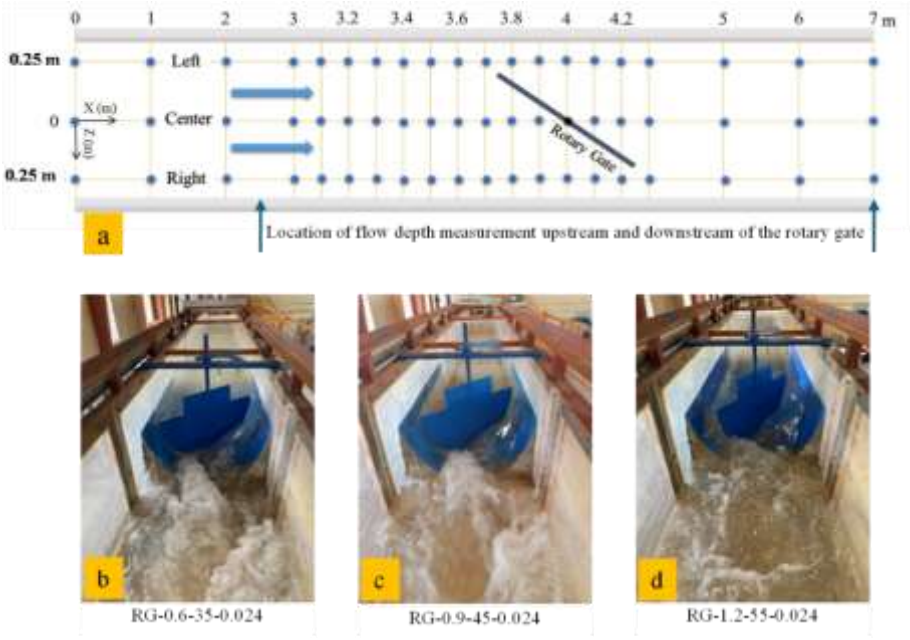

2.2 Dimensional analysis

The geometric, kinematic, and dynamic variables that affect the hydraulics of the rotary gate flow under free-flow conditions are shown in Table 1.

Table 1 Units and dimensions of the variables impacting the rotary gate

Variable Name	Variable Symbol	Unit	Dimension
Transition length	L_T	m	L
The opening angle of the gate relative to the transverse direction (opening angle)	θ	-	-
Water surface width *	W_T	m	L
Flow rate	Q	cubic meters per second	$L^3 T^{-1}$
The depth upstream of the gate	y_1	m	L
Depth downstream of the gate	y_2	m	L
Gravitational acceleration	g	meters per second squared	LT^{-2}
The specific mass of the fluid	ρ	kg/m^3	ML^{-3}
Fluid dynamic viscosity	μ	kg/m/s	$ML^{-1} T^1$
Surface tension	σ	Newton per meter	MT^{-2}

*Width of the water surface (W_T) denotes the sum of the water surface width on the left side (W_L) and the right side of the gate (W_R) at the place of flow drop

In free-flow conditions, the general function is as Eq. 1(Karami et al., 2020):

$$F(L_T,\theta,Q,y_1,W_T,g,\rho,\mu,\sigma)=0 \quad (1)$$

Using Buckingham's π theorem, three variables y_1, Q, and ρ are selected as repeating variables. The general function, including dimensionless parameters, can be expressed as Eq. 2 (White, 2009):

$$F(\frac{L_T}{y_1},\theta,\frac{W_T}{y_1},\frac{gy_1^5}{Q^2},\frac{\mu y_1}{\rho Q},\frac{\sigma y_1^3}{\rho Q^2})=0 \quad (2)$$

It can be concluded from Eq. (2) that:

$$F(\frac{L_T}{y_1},\theta,\frac{W_T}{y_1},\frac{Q^2}{gy_1^5},\frac{1}{Re},\frac{1}{We})=0 \quad (3)$$

Eq. (3) can be written in the form of Eq. (4):

$$\frac{Q^2}{gy_1^5}=\phi(\frac{L_T}{y_1},\theta,\frac{W_T}{y_1},\frac{1}{Re},\frac{1}{We}) \quad (4)$$

In these equations, *We* and *Re* represent the Weber and Reynolds numbers of the flow upstream of the gate, respectively. In this research, due to the presence of a flow with a depth greater than 0.05 m, the Weber number has been neglected. Also, considering that the Reynolds number is more than 4000 in all experiments, the effect of this parameter has been ignored. Therefore, it can be concluded:

$$\frac{Q^2}{gy_1^5}=\phi(\frac{L_T}{y_1},\theta,\frac{W_T}{y_1})\Rightarrow Q=\phi(\frac{L_T}{y_1},\theta,\frac{W_T}{y_1}).\sqrt{gy_1^5} \quad (5)$$

From Eq. 5, it follows that the discharge coefficient of the gate under free-flow conditions is a function of three dimensionless parameters: the ratio of the length of the transition to the flow depth upstream of the gate, the opening angle of the gate, and the ratio of the water surface width to the flow depth upstream of the gate. Equation 6 can be derived from Eq. 5.

$$C_{dF}=\phi(\frac{L_T}{y_1},\theta,\frac{W_T}{y_1}) \quad (6)$$

2.3 Range of geometric and hydraulic variables

In this research, due to the importance of discharge in determining the water level upstream and downstream of the gate, the discharge varied from 0.020 to 0.038 m^3/s with an increase of 0.002 m^3/s. The opening angle of the gate was adjusted from 35 to 85 degrees in 5-degree intervals. Table 2 shows the nomenclature of the tests and the range of changes of the different geometric and hydraulic variables used in this study, the flow depth at a distance of 1.5 meters upstream of the gate is defined as the upstream depth (y_1), and the depth of 3 m downstream from the gate axis is defined as the downstream depth (y_2).

Table 2 List of experiments performed

L_T (m)	θ°	Q ($m^3.s^{-1}$)	y_1 (m)	W_T (m)	Upstream Froude number	No. Exp	Abbreviations
0.6	35	0.020-0.030	0.226-0.288	0.110-0.114	0.099-0.103	6	RG-0.6-θ-Q
	40	0.020-0.034	0.210-0.288	0.141-0.146	0.111-0.117	8	
	45		0.185-0.268	0.177-0.183	0.134-0.146	10	
	50		0.172-0.248	0.216-0.219	0.149-0.164	10	
	55		0.155-0.225	0.256-0.259	0.174-0.190	10	
	60		0.145-0.207	0.294-0.298	0.193-0.215	10	
	65	0.020-0.038	0.134-0.191	0.332-0.342	0.217-0.242	10	
	70		0.127-0.179	0.369-0.385	0.235-0.267	10	
	75		0.123-0.169	0.408-0.429	0.247-0.291	10	
	80		0.120-0.162	0.448-0.472	0.256-0.310	10	
	85		0.117-0.159	0.488-0.517	0.266-0.319	10	
0.9	35	0.020-0.026	0.239-0.281	0.110-0.112	0.091-0.093	4	RG-0.9-θ-Q
	40	0.020-0.030	0.221-0.257	0.142-0.144	0.102-0.106	6	

L_T (m)	θ°	Q ($m^3.s^{-1}$)	y_1 (m)	W_T (m)	Upstream Froude number	No. Exp	Abbreviations
	45		0.195-0.287	0.176-0.178	0.124-0.132	10	
	50		0.179-0.264	0.213-0.216	0.141-0.149	10	
	55		0.162-0.238	0.250-0.257	0.163-0.171	10	
	60		0.152-0.221	0.287-0.299	0.183-0.195	10	
	65	0.020-0.038	0.135-0.202	0.320-0.342	0.215-0.223	10	
	70		0.128-0.187	0.356-0.384	0.232-0.250	10	
	75		0.126-0.176	0.396-0.427	0.238-0.274	10	
	80		0.121-0.170	0.435-0.471	0.253-0.289	10	
	85		0.120-0.166	0.477-0.515	0.256-0.299	10	
	35	0.020-0.026	0.254-0.298	0.109-0.111	0.083-0.085	4	
	40	0.020-0.030	0.233-0.300	0.140-0.142	0.095-0.097	6	
	45		0.203-0.292	0.175-0.176	0.116-0.128	10	
	50		0.189-0.271	0.211-0.216	0.130-0.143	10	
	55		0.171-0.244	0.246-0.258	0.151-0.168	10	
1.2	60		0.160-0.226	0.283-0.298	0.166-0.188	10	RG-1.2-θ-*Q*
	65	0.020-0.038	0.146-0.205	0.319-0.340	0.191-0.218	10	
	70		0.138-0.193	0.355-0.382	0.208-0.239	10	
	75		0.130-0.181	0.391-0.425	0.227-0.263	10	
	80		0.125-0.173	0.430-0.467	0.241-0.281	10	
	85		0.129-0.168	0.469-0.510	0.250-0.294	10	

3. Results and Discussion

3.1 Water level variations along the canal

To analyze the water level profile in this research, measurements were taken along a 7 m section, from 4 m upstream of the gate axis to 3 m downstream. In addition, to investigate the lateral changes in the water level profile, measurements were taken at three cross-sections and along the longitudinal direction of the canal: the center, the left side, and the right side of the rotary gate. Fig. 4 shows the lateral changes of the water level profile for the maximum discharge and different gate opening angles of 45, 65, and 85 degrees, respectively, with a transition length of 0.9 m.

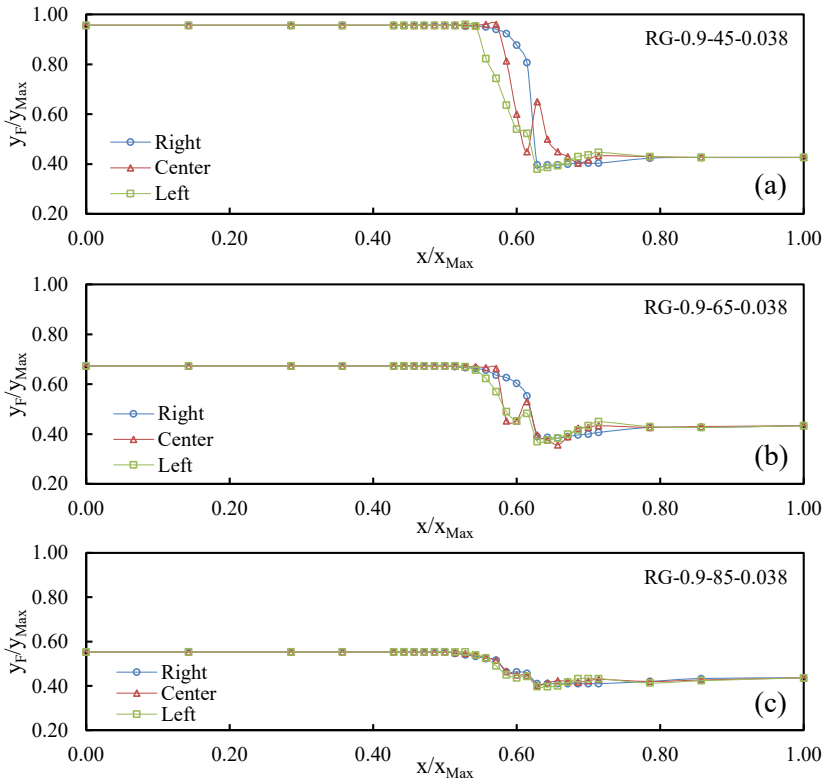

Fig. 4 water level profile variation at L_T=0.9 *m*: a) 45° , b) 65°, and c) 85°

From the profiles, it can be seen that the lateral changes in the water level decrease as the opening angle of the rotary gate increases. In other words, the most significant lateral changes in the water level profile occur at a 35-degree opening angle, while the smallest changes are associated with an 85-degree angle.

3.2 Impact of rotary gate opening angle on water level profile in free flow conditions

To assess the impact of varying the gate opening angle on the water level profile under free-flow conditions, Fig. 5 illustrates the changes in water level profiles at different gate opening angles for transitions with lengths of 0.6, 0.9, and 1.2 m, respectively. It can be seen that as the opening angle of the rotary gate is increased, the upstream water depth is reduced. Also, as the opening angle increases, the magnitude of the water level fluctuations downstream of the gate reduces. As can be seen from Fig. 5, the increase in the gate opening angle initially leads to significant changes in the depth upstream of the rotary gate. However, as the opening angle increases further, the upstream flow depth reduces at a diminishing rate. For instance, when the opening angle is adjusted from 35 degrees to 40 degrees, the change in upstream flow depth is much greater than when the angle is changed from 80 degrees to 85 degrees. This trend holds for all transitions with lengths of 0.6, 0.9, and 1.2 m. In addition, Fig. 5 shows that, assuming a constant discharge and opening angle, the upstream flow depth decreases as the length of the transition decreases. On the other hand, the flow depth at the upstream section increases with a longer transition.

Fig. 5 The water level profile changes at various opening angles: L_T= 0.6 *m*, b) L_T= 0.9 *m*, c) L_T= 1.2 *m*

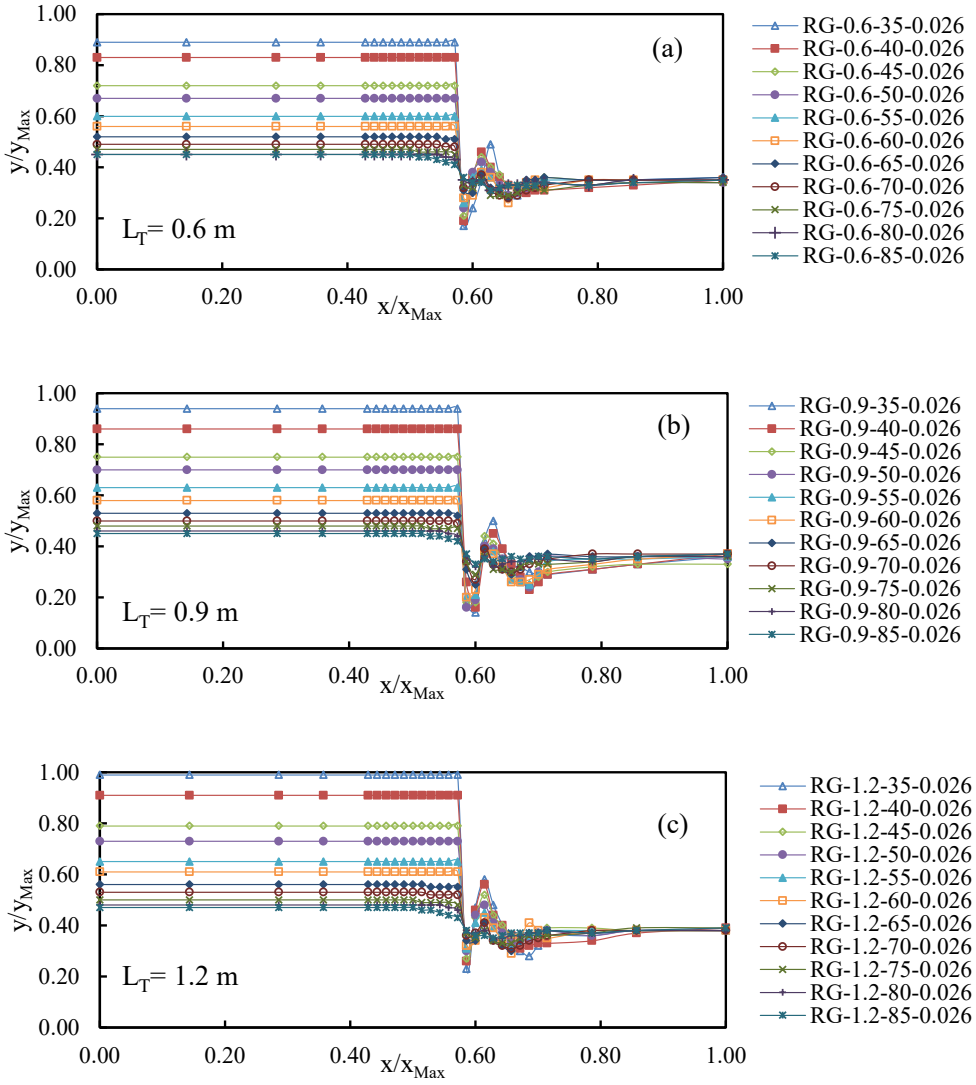

3.3 Stage-discharge relationship under free flow conditions

The stage-discharge (Q-y_1) method uses a general equation in which the flow passing through the structure is a function of the upstream flow depth (Eq. 7). Where Q is flow discharge, y_1 is upstream flow depth, and κ and ω coefficients that are dependent on the gate opening angle and transition length. Given the known upstream depth in various discharges, different opening angles, and transition lengths, the Q-y_1 curves for a rotary gate were plotted in Fig. 6. These diagrams enable one to determine the constant coefficients in the Q-y_1 equation for each gate opening angle. As shown, the Q-y_1 curves follow exponential equations. The coefficients and exponents vary depending on the opening angle. Also, these coefficients vary with changes in the transition length.

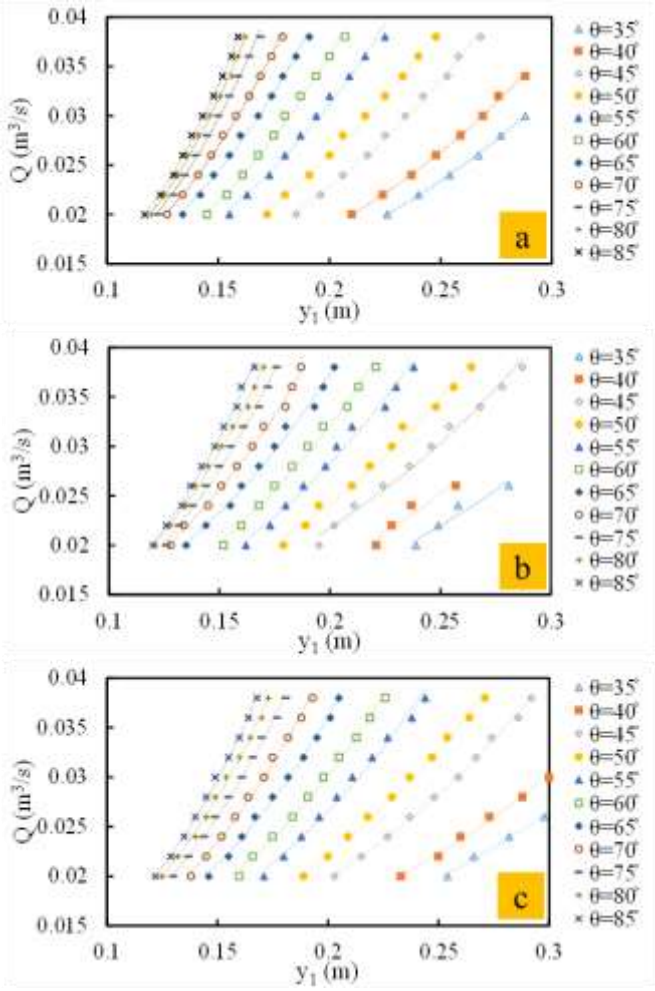

Fig. 6 Q-y_1 for transition with length: a) 0.6 *m*, b) 0.9 *m*, c) 1.2 *m*

After extracting the coefficient and power values for the Q-y_1 equation for different opening angles and transitions, the changes in these coefficients were examined with respect to the opening angle and transition length. Finally, Eq. 7 was put forward to calculate the discharge as a function of transition length.

$$Q = \kappa y_1^{\omega} \tag{7}$$

If L_T=0.6 *m*:

$$\kappa = 0.0521 e^{2.4546\,\theta} \tag{8}$$

$$\omega = 0.5148\,\theta^2 - 0.5439\,\theta + 1.8256 \tag{9}$$

If L_T=0.9 *m*:

$$\kappa = 0.0536\, e^{2.1107\,\theta} \tag{10}$$

$$\omega = 0.8685\,\theta^2 - 1.4381\,\theta + 2.1980 \tag{11}$$

And if L_T=1.2 *m*:

$$\kappa = 0.0469 e^{2.3617\,\theta} \tag{12}$$

$$\omega = -0.117\,\theta^2 + 0.7018\,\theta + 1.2329 \tag{13}$$

where, θ is in radians. Using all data obtained from the experiments, Eqs. 14 and 15 were extracted to compute the coefficient and the power of the Stage-discharge equation.

$$\kappa = -0.619 + 1.514\,\theta - 0.291\,L_T \tag{14}$$

$$\omega = 1.365 + 0.457\,\theta - 0.048\,L_T \tag{15}$$

It should be noted that the accuracy of Eqs. 7 and 8-13, which gives the individual relationships for the coefficients κ and ω for each transition, is much higher than that of Eqs. 7, 14, and 15, where these coefficients are determined as functions of the opening angle and the transition length. To evaluate the accuracy of the different methods for calculating the constant coefficients in the Q-y_1 equations, Fig. 7 is presented. This figure compares the constant coefficients calculated from the laboratory data (Geometric symbols such as the triangle (▲) and the square (■)) with the constant coefficients calculated from Eqs. 7 and 8-13 (Continuous curved lines), which provide separate relationships for the constant coefficients κ and ω for each transition. Furthermore, the coefficients obtained from Eqs. 14 and 15 that take the gate opening angle and the transition length into consideration (Dashed lines) are also presented. As evident from this figure, the method of calculating the constant coefficients of the Q-y_1 relation by treating each transition separately yields more accurate estimates.

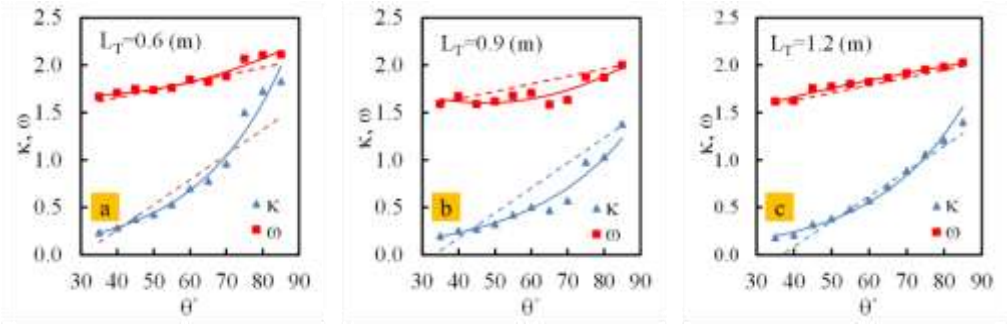

Fig. 7 Comparing the accuracy of estimating the constant coefficients of ω and k' by using Eqs. 8-13 and Eqs. 14-15: a) L_T= 0.6 *m*, b) L_T= 0.9 *m*, c) L_T= 1.2 *m*

3.4 Derivation of the flow discharge equation using dimensionless parameters

Using dimensionless parameters, Eq. 16 is derived to generalize the Q-y_1 relationship for different geometric scales.

$$Q = \phi(\frac{L_T}{y_1}, \cos\theta, \frac{W_T}{y_1}).\sqrt{gy_1^5} \Rightarrow Q = C_{dF}.\sqrt{gy_1^5} \qquad (16)$$

The flow discharge depends on three dimensionless parameters; once the upstream depth is known for various discharges, the opening angles and different transitions of the desired dimensionless parameters can be determined. based on the following relationships, the variation of these parameters concerning the discharge is shown in Fig. 8.

$$\frac{L_T}{y_1} = L_{T*} \qquad (17)$$

$$\frac{W_T}{y_1} = W_{T*} \qquad (18)$$

Fig. 8: a-f: The effect of dimensionless parameters on the discharge coefficient, g: The effect of varying transition length on the discharge coefficient of the rotary gate

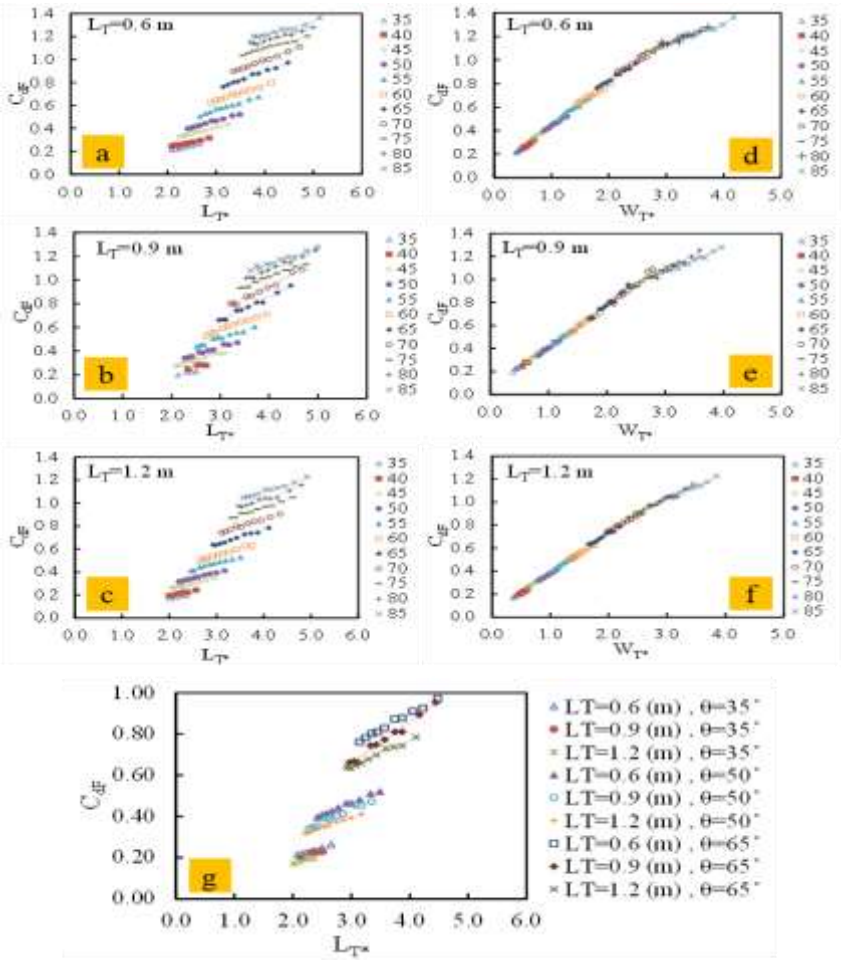

Fig. 8 shows that: the discharge coefficient increases in the free flow state as the opening angle of the gate increases, which in turn widens the water surface. The highest discharge coefficient is observed at an opening angle of 85 degrees (corresponding to the largest water surface width), while the lowest discharge coefficient is at an opening angle of 35 degrees (which has the smallest water surface width). Additionally, Fig. 8a-8f indicate that as the ratio of the transition length to the upstream flow depth increases, the discharge coefficient increases. To examine the effect of L_T on the discharge coefficient, Fig. 8g is presented. This figure clearly shows that, for a fixed opening angle, the higher discharge coefficient corresponds to the rotary gate with a transition length of 0.6 m, while the lowest discharge coefficient is associated with a transition length of 1.2 m. This indicates that as the length of the transition increases, the discharge coefficient decreases. In summary, it can be concluded that increasing the gate opening angle or decreasing the transition length results in a higher discharge coefficient. Conversely, decreasing the opening angle or increasing the transition length leads to a lower discharge coefficient. Using dimensional analysis, a mathematical relationship has been proposed to predict the discharge coefficient of the rotary gate. The study found that the C_{dF} is influenced by three dimensionless parameters L_{T*}, W_{T*}, and θ. The equation is as follows:

$$C_{dF} = 0.992^{\eta}(\psi)\eta^{0.571} \qquad (R^2 = 0.98) \tag{19}$$

that η and ψ are determined by Eqs. 20 and 21 respectively.

$$\eta = L_{T*}W_{T*}\theta \tag{20}$$

$$\psi = 4.723e^{-0.903 L_T} \qquad (R^2 = 0.99) \tag{21}$$

The discharge coefficient values calculated using laboratory data and those calculated using Eq. 19 are compared in Fig. 9. The scatter of points relative to the 45-degree line demonstrates a high correlation between the experimental and calculated values. The discharge coefficient of the rotary gate varies with the gate opening angle: 0.18–1.35 for a 0.6 m transition, 0.17–1.29 for a 0.9 m transition, and 0.15–1.23 for a 1.2 m transition.

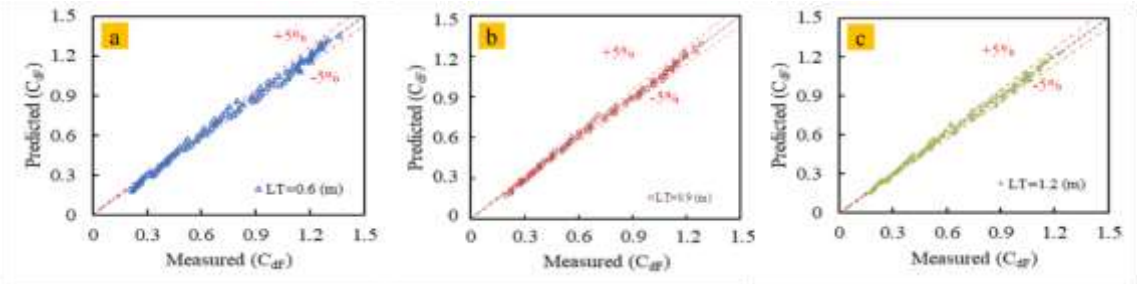

Fig. 9 Comparison of the discharge coefficient calculated using laboratory data versus the values calculated using Eq. 19: a*) L_T=0.6 m, b) L_T=0.9 m, c) L_T=1.2 m*

3.4.1 Numerical example

Equation 19, developed for estimating the discharge coefficient under free-flow conditions, expresses the coefficient as a function of the dimensionless parameters W_{T*}, L_{T*}, and θ. To demonstrate its application, consider a laboratory test scenario with the following parameters:

- Transition length: L_T=0.6 *m*
- Measured discharge (actual flow rate): Q=0.02 $m^3.s^{-1}$
- Upstream water depth: y_1=0.185 *m*
- Dimensionless parameters: W_{T*}=0.987, L_{T*}=3.243, and θ=0.785 *rad*. By substituting these values into the empirical Eq. 19, the discharge coefficient and corresponding discharge can be estimated.

$$C_{dF} = 0.992^{\eta}(\psi)\eta^{0.571} = 0.992^{2.513} \times 0.252 \times 2.513^{0.571} = 0.418$$

$$\psi = 4.723e^{-0.903 L_T} = 4.723e^{-0.903 \times 3.243} = 0.252$$

$$\eta = L_{T*}W_{T*}\theta = 0.987 \times 3.243 \times 0.785 = 2.513$$

$$Q = C_{dF}.\sqrt{g y_1^5} = 0.418 \times \sqrt{9.806 \times 0.185^5} = 0.0193 \approx 0.02 \ \ m^3.s^{-1}$$

The comparison indicates that Eq. 19 provides a reliable estimation, showing good agreement with the measured discharge value.

3.5 Effect of transition length on flow coefficient and equation accuracy

After the flow enters the rectangular canal, it moves toward the gate and divides into two parts upon hitting its edge. This division creates two water surface widths (W_R and W_L) and two cross-sections (A_R and A_L) at the sides of the gate. The right-side cross-section always sits on the semi-circular section of the transition, while the left-side cross-section is located on the gradual transition. Since the right cross-section is on the semi-circular transition, changes in the length of the gradual transition upstream have no effect on it and depend only on the flow depth and the opening angle of the rotary gate. However, the left cross-section is dependent on the changes in the length of the gradual transition and the opening angle, meaning its area changes throughout the gradual transition. In other words, the left cross-section is a function of the transition length in

addition to the flow depth and opening angle. Calculations have shown that as the length of the transition decreases, the left cross-section increases, and conversely, as the length of the transition increases, this cross-section decreases.In other words, as the length of the transition increases, the cross-section of the flow gradually transforms from rectangular to semi-circular, resulting in the left cross-section being smaller than when the transition length is shorter. These data indicate that under the same hydraulic and geometric conditions (constant discharge and angle), a decrease in the length of the transition leads to an increase in both the output cross-section and the width of the water surface. Therefore, the main reason for the increase in the discharge coefficient of the gate with a decrease in the length of the transition is related to the changes in the left cross-section and water width, increasing these parameters in the output flow from the gate. As shown in Eq. 19, the discharge coefficient has a direct relationship with the width of the water surface.

To investigate the effect of transition length on the discharge coefficient of the rotary gate in free flow conditions, the dimensionless parameter ($L_T/y_1=L_{T*}$) was excluded from the dimensional analysis, and Eq. 22 was derived without considering the effect of the transition length to calculate the discharge coefficient.

$$C_{dF} = 0.4822(0.9521)^{\eta'}(\eta')^{0.7122} \quad (22)$$

$$\eta' = \theta \times W_{T*} \quad (23)$$

The comparison of Eq. 22 with Eqs. 7 and 19 in Fig. 10 reveal that the transition length significantly affects the rotary gate's discharge coefficient. Ignoring this effect increases the error in calculating both the discharge coefficient and the discharge. In Fig. 10, Q_1 is the discharge from Eq. 7, Q_2 from Eq. 19, and Q_3 from Eq. 22. Thus, neglecting the transition length effect greatly amplifies the estimation errors of discharge. Eq. 24 was used to calculate the error of the equations proposed for discharge estimation.

$$Error\ (\%) = \frac{|Q - Qc|}{Q} \times 100 \quad (24)$$

In this equation, Q_c represents the discharge calculated from one of Eqs. 7, 19, or 22, while Q denotes the actual discharge.

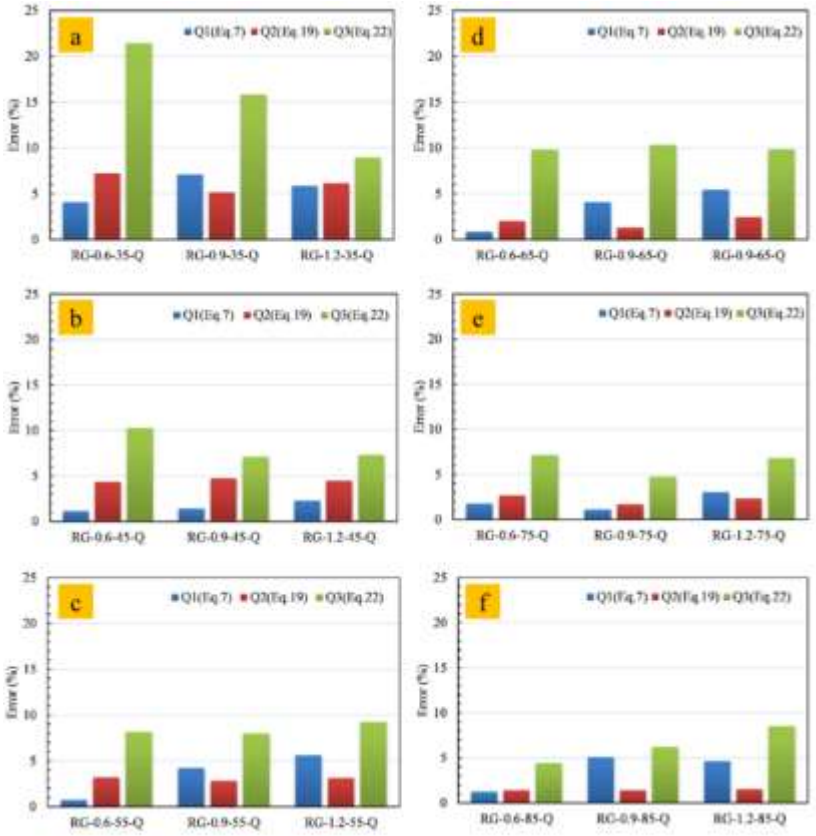

Fig. 10 Error percentage of Eqs. 7, 19 and 22: a) *θ=35˚, b) θ=45˚, c) θ=55˚, d) θ=65˚, e) θ=75˚, f) θ=85˚*

3.6 Accuracy comparison of flow-discharge measurement methods

The Stage-discharge results obtained from Eqs. 7, 16, and the experimental discharges have been compared. The results show that the discharge calculated from Eq. 16 provides a more accurate result than the Q-y_1 Equation (Eq. 7). However, this does not mean that the Q-y_1 relationship is not accurate. Therefore, it can be concluded that both relations, those obtained for the calculation of the rotary gate discharge under free flow conditions, provide sufficient accuracy. To evaluate the performance of Eqs. 7 and 16, the discharges, Q_c, were computed based on Eqs. 7 and 16, and compared to the observed values, Q. Also, indices such as the average relative error, *ARE*, root mean square error, *RMSE*, standard error, *SE*, and normal root mean square error, *NRMSE*, are defined by Eqs. 25-28 (Marashi et al. (2021a)), were respectively computed and tabulated in Table 3.

$$ARE = \frac{\sum \left| \frac{Q - Q_c}{Q} \right|}{N} \times 100 \quad (25)$$

$$RMSE = \sqrt{\frac{\sum (Q - Q_c)^2}{N - 1}} \quad (26)$$

$$SE = \frac{RMSE}{\bar{Q}} \times 100 \quad (27)$$

$$NRMSE = \frac{RMSE}{Q_{max} - Q_{min}} \times 100 \quad (28)$$

Table 3 shows that the relationship proposed based on the first approach (Eq. 16) presented better performance than Eq. 7.

Table 3 Error analysis of the different discharge equations

Approach	ARE (%)	RMSE ($m^3. s^{-1}$)	SE (%)	NRMSE (%)
Eq. (7)	3.84	0.00142	4.96	7.87
Eq. (16)	2.12	0.00084	2.93	4.65

3.7 Comparison of the study results with other similar studies

Marashi et al. (2019 and 2021a) investigated the behavior of the rotary gate in the semicircular canal, focusing on how variations in gate opening angles affect flow characteristics. Their results indicated that increasing the gate opening angle leads to a higher discharge coefficient, demonstrating a direct relationship between gate position and fluid discharge. Similarly, the present study confirmed this trend, showing that the discharge coefficient increases as the rotary gate opening angle is enlarged, which aligns with the findings of Marashi and colleagues and supports the consistency of flow behavior under varying gate configurations. However, it is important to note that while Marashi et al.'s studies were conducted in semicircular canals, the present research focused on a rotary gate in a rectangular canal. Additionally, a gradual transition approach was employed in the current study to better capture the effects of progressive changes in gate position. Due to the more complex flow patterns and turbulence characteristics in open rectangular canals, a direct and detailed comparison with Marashi et al.'s results is limited. Nevertheless, the consistency in the overall trend of increasing discharge coefficient with larger gate openings reinforces the general applicability of their findings and highlights the relevance of gate opening angle as a key parameter influencing flow behavior across different canal geometries.

4. Conclusion

This study investigated the hydraulic performance of a semi-circular rotary gate in a rectangular canal. The results indicated that this gate, with its unique features such as requiring minimal force for operation, symmetrical distribution of flow forces on both sides, and reduced issues with sediment accumulation and floating debris,' can serve as a suitable alternative to traditional gates in irrigation networks. Laboratory studies revealed the following:

1. The discharge coefficient (C_d) significantly increased as the gate opening angle increased from 35° to 85°, rising from approximately 0.6 to 0.9. Additionally, reducing the transition length from 1.2 m to 0.6 m led to an increase in the discharge coefficient.

2. The mathematical relationships presented in this study, derived through dimensional analysis and experimental data, demonstrated high accuracy in predicting the discharge coefficient. For example, a comparison of experimental and computational results showed that data dispersion was close to the 45° line, with a mean relative error of less than 5%.

3. The removal of the transition length parameter from the dimensional analysis under free flow conditions led to the derivation of a simplified equation. Comparison with the full equations, which consider the transition length, showed that ignoring this parameter causes significant errors in estimating both discharge and the discharge coefficient.

4. Ultimately, this research demonstrated that the use of a semi-circular rotary gate in rectangular canals, provided that it is designed and installed accurately, can enhance hydraulic efficiency and improve the accuracy of flow measurement. The findings of this study can serve as a useful tool in the design and optimization of irrigation systems and water resource management.

This study was conducted at a laboratory scale and only under free-flow conditions, within a limited range of discharge and gate opening angles, on a Plexiglas canal with a specific transitional cross-section. Therefore, its results require verification and recalibration when applied to real channels, different cross-sections or materials, submerged flow conditions, and sediment deposition. Despite these limitations, the proposed relationships can be effectively used in the design, calibration, and optimization of rotary gates and flow control in irrigation networks with similar conditions, especially under free-flow conditions.

Statements and Declarations

Data availability

Data will be made available on request.

Conflicts of interest

The authors of this paper declared no conflict of interest regarding the authorship or publication of this paper.

Author contribution

M. Kheiraie: Physical model construction, Measurement and data collection & data analysis; H. Yonesi: Analysis, interpretation and description of charts & manuscript editing; B. Shahinejad: statistical analysis; H. Torabipoodeh: Review and editing; A. Marashi: Validation and data curation.

AI Use Declaration

During the preparation of this work, the author(s) used ChatGPT to improve some sentences. The authors have

thoroughly reviewed and revised the content as necessary and assumed full responsibility for the final manuscript.

References

Belaud, G., Cassan, L., & Baume, J. P. (2009). Calculation of contraction coefficient under sluice gates and application to discharge measurement. *Journal of Hydraulic Engineering, 135*(12), 1086–1091. https://doi.org/10.1061/(ASCE)HY.1943-7900.0000122

Bijankhan, M., Ferro, V., & Kouchakzadeh, S. (2013). New stage-discharge relationships for radial gates. *Journal of Irrigation and Drainage Engineering, 139*(5), 378–387. https://doi.org/10.1061/(ASCE)IR.1943-4774.000055

Daneshfaraz, R., Ghahramanzadeh, A., Ghaderi, A., Rezazadeh Joudi, A., & Abraham, J. (2016). Investigation of the effect of edge shape on characteristics of flow under vertical gates. *Journal of the American Water Works Association, 108*(8), 425–432. https://doi.org/10.5942/jawwa.2016.108.0102

Daneshfaraz, R., Norouzi, R., Ebadzadeh, P. (2022). Experimental and numerical study of sluice gate flow pattern with non-suppressed sill and its effect on discharge coefficient in free-flow conditions. *Journal of Hydraulic Structures, 8*(2), 17517. 10.22055/jhs.2022.40089.1201

Dehghani, F., Hosseini, S. H., Najarzadeh, S. (2023). Experimental study of discharge coefficient of U-shaped sluice gate under free and submerged flow conditions. *Journal of Hydraulic and Water Engineering, 9*(3), 2751. 10.22044/jhwe.2023.12315.1001

Gharibreza, M., Nasrollahi, A., Afshar, A., Amini, A., & Eisaei, H. (2018). Evolutionary trend of the Gorgan Bay (southeastern Caspian Sea) during and post the last Caspian Sea level rise. *Catena, 166*, 339–348. https://doi.org/10.1016/j.catena.2018.04.016

Hashem, T., Mohammed, A. Y., & Alfatlawi, T. J. (2024). Hydraulic characteristics of labyrinth sluice gate. *Flow Measurement and Instrumentation, 96*, 102556. https://doi.org/10.1016/j.flowmeasinst.2024.102556

Karami Moghadam, M., Amini, A., & Keshavarzi, A. (2020). Intake design attributes and submerged vanes effects on sedimentation and shear stress. *Water and Environment Journal*, 34(3), 374–380. https://doi.org/10.1111/wej.12471

Khalili Shayan, H., Farhoudi, J., & Vatankhah, A. R. (2021). Solutions for estimating opening of sluice and radial gates for flow regulation. *Journal of Irrigation and Drainage Engineering, 147*(3), 06021001. https://doi.org/10.1061/(ASCE)IR.1943-4774.0001541

Kim, D. G. (2007). Numerical analysis of free flow past a sluice gate. *Journal of Civil Engineering, 11*(2), 127–132. https://doi.org/10.1007/BF02823856

Lauria, A., Calomino, F., Alfonsi, G., & D'Ippolito, A. (2020). Discharge coefficients for sluice gates set in weirs at different upstream wall inclinations. *Water, 12*(1), 245. https://doi.org/10.3390/w12010245

Marashi, A, Kouchakzadeh, S., Yonesi, H. (2023). Rotary gate discharge determination for inclusive data from free to submerged flow conditions using ENN, ENN-GA, and SVM-SA. *Journal of Hydroinformatics, 25*(4), 1312–1328. https://doi.org/10.2166/hydro.2023.202

Marashi, A. (2019). *Hydraulics of butterfly gate: Determination of specifications and application criteria in the canal* (Ph.D. Thesis, University of Lorestan). 126 pp.

Marashi, A., Kouchakzadeh, S., Rashidi, N., & Yonesi, H. (2021b). Rotary gate: Submerged flow condition. *Flow Measurement and Instrumentation, 81*, 102035. https://doi.org/10.1016/j.flowmeasinst.2021.102035

Marashi, A., Kouchakzadeh, S., Yonesi, H., & Torabi-Poudeh, H. (2021a). Hydraulics of a rotary gate: Novel structure for semicircular canals. *Journal of Irrigation and Drainage Engineering, 147*(5), 04021007. https://doi.org/10.1061/(ASCE)IR.1943-4774.0001537

Meng, W., Li, L., Zhao, S., & Li, P. (2024). Flow regime discrimination and methodology for calculating discharge in trapezoidal sluice gates. *Flow Measurement and Instrumentation, 100*, 102710. https://doi.org/10.1016/j.flowmeasinst.2024.102710

Rojas, S. (2020). Determination of the discharge coefficient of a heavy hydraulic head slide gate. *Revista de Investigación de Física, 23*(3), 20316.

Salmasi, F., & Abraham, J. (2020). Expert system for determining discharge coefficients for inclined slide gates using genetic programming. *Journal of Irrigation and Drainage Engineering, 146*(12), 06020013. https://doi.org/10.1061/(ASCE)IR.1943-4774.0001520

Swamee, P. K. (1992). Sluice-gate discharge equations. *Journal of Irrigation and Drainage Engineering, 118*(1), 56–60. https://doi.org/10.1061/(ASCE)0733-9437(1992)118:1(56)

Vanden-Broeck, J. (1997). Numerical calculations of the free-surface flow under a sluice gate. *Journal of Fluid Mechanics, 330*, 339–347. https://doi.org/10.1017/S0022112096003849

Wang, L., & Diao, M. (2021). Discharge coefficient and head loss under sluice gates with small opening. *Journal of Irrigation and Drainage Engineering, 147*(3), 04020067. https://doi.org/10.1061/(ASCE)IR.1943-4774.0001627

White, F. M. (2009). *Fluid mechanics* (7th ed.). New York, NY: McGraw-Hill. University of Rhode Island.

© Authors, Published by Journal of *Environment and Water Engineering*. This is an open-access article distributed under the CC BY (license http//creativecommons.org.licenses.by.4.0).